African Journal of Advanced Pure and Applied Sciences (AJAPAS)
Online ISSN: 2957-644X
Volume 5, Issue 1, 2026
Page No: 194-204
Website: https://aaasjournals.com/index.php/ajapas/index
ISI 2025: 1.126 SJIFactor 2024: 6.752 معامل التأثير العربي: 1.62

Performance Evaluation of a GWO-Optimized PID Controller for DC Motor System

Mohammed W. Bilhasan [1 *], Adel Agila [2] , Mohammed M. Syam [3]
[1,3] Department of Mechanical Engineering, Faculty of Engineering, University of Derna, Derna, Libya
[2] Departments of Mechanical Engineering, Omar Al Mukhtar university, Faculty of Engineering, Al-Bayda, Libya

تقييم أداء وحدة التحكم (PID) المحسّنة بخوارزمية "ذئب الرمادي" لنظام محرك التيار المستمر

محمد بالحسن [1*]، عادل عقيلة [2]، محمد صيام [3]
[3،1] قسم الهندسة الميكانيكية، كلية الهندسة، جامعة درنة، درنة، ليبيا
[2] قسم الهندسة الميكانيكية، كلية الهندسة، جامعة عمر المختار، البيضاء، ليبيا

[*]Corresponding author: mohammedwanees93@gmail.com

Received: November 13, 2025	Accepted: January 21, 2026	Published: February 04, 2026

Abstract:
A classic control method and a modern optimization approach were combined in this research to better address industrial needs. A DC motor was chosen for its flexibility and ease of control, and a model was developed to assess performance under various conditions. Rather than relying on manual tuning, an advanced algorithm was used to adjust the controller settings, and accuracy was measured with a trusted indicator. With this approach, faster and more accurate results were achieved compared to traditional methods. Overall, the use of the Grey Wolf Optimization (GWO) approach not only made the system faster but also noticeably more accurate compared to previous methods. When compared to other optimization methods, including the Genetic Algorithm (GA) and Particle Swarm Optimization (PSO), further performance benefits were demonstrated. The response of the controller remained within the designated design parameters, with errors reduced to the lowest level. These results demonstrate that employing GWO with ITAE-based tuning offers a robust and efficient solution for industrial motor control, ensuring both rapid responsiveness and reliable stability.

Keywords*:* DC-motor, PID controller, Grey Wolf Optimization (GWO), fractional derivative, Integral Time Absolute Error (ITAE) , Integrated Absolute Error (IAE).

الملخص
جمعت هذه الدراسة بين طرق التحكم الكلاسيكية وأساليب التحسين الحديثة لتلبية المتطلبات الصناعية بشكل أفضل. وقد وقع الاختيار على محرك التيار المستمر (DC motor) نظراً لمرونته وسهولة التحكم فيه، حيث تم تطوير نموذج لتقييم الأداء تحت ظروف تشغيلية متنوعة. وبدلاً من الاعتماد على الضبط اليدوي التقليدي، تم توظيف خوارزمية متطورة لضبط إعدادات وحدة التحكم، مع قياس الدقة باستخدام مؤشر موثوق. وبفضل هذا النهج، تم تحقيق نتائج أسرع وأكثر دقة مقارنة بالطرق التقليدية.
وبشكل عام، فإن استخدام خوارزمية "تحسين ذئب الرمادي" (GWO) لم يساهم في زيادة سرعة استجابة النظام فحسب، بل أدى أيضاً إلى تحسن ملحوظ في الدقة مقارنة بالأساليب السابقة. وعند مقارنة النتائج مع طرق التحسين الأخرى، بما في ذلك الخوارزمية الجينية (GA) وخوارزمية تحسين سرب الجسيمات (PSO)، أثبتت النتائج تفوقاً إضافياً في الأداء. كما ظلت استجابة وحدة التحكم ضمن معايير التصميم المحددة، مع خفض الأخطاء إلى أدنى مستوياتها. وتؤكد هذه النتائج أن دمج خوارزمية (GWO) مع معيار ضبط (ITAE) يقدم حلاً قوياً وفعالاً للتحكم في المحركات الصناعية، مما يضمن استجابة سريعة واستقراراً موثوقاً في آن واحد.

الكلمات المفتاحية :محرك التيار المستمر، وحدة التحكم (PID)، خوارزمية تحسين ذئب الرمادي (GWO)، المشتق الكسري، تكامل القيمة المطلقة للخطأ المضروب في الزمن (ITAE)، تكامل القيمة المطلقة للخطأ (IAE).

Introduction

Direct current (DC) motors are electromechanical converters of electric energy into mechanical rotational motion through the fundamental principles of electromagnetism. The fundamental working includes supply of direct current that interacts with a magnetic field to develop a mechanical torque to turn the motor shaft. The mechanism is founded on the Lorentz force, whereby a conductor carrying an electric current placed in a magnetic field experiences a force. The continuous application of this force, facilitated by the interior components of the motor, allows for continuous rotation [1].

DC motors have been and are still crucial elements in many industrial control systems due to their inherent advantages. Some of these include a high capability of generating high starting torque, which allows them to efficiently power heavy loads. Their capability to respond to high speed allows for the possibility of having dynamic and precise control in high-demand applications. In addition, their relatively small size and weight make them portable and simple to implement in many systems. The fact that DC motors can be used in many control tuning methods provides versatility in modifying their performance to meet a particular operating need [2].

Due to these desirable characteristics, DC motors have been used throughout several modern applications. These include such critical applications as robotics, where precise and controlled motion is called for; electric vehicles, utilizing their high starting torque to drive vehicles; disk drives, requiring precise speed control; machine tools, calling for powerful, controllable drives; and servo-valve actuators, where precision positioning is needed. The Direct Electrical Energy to Mechanical Rotation principle underlies DC motors to render them a base technology in most electromechanical applications [2,3].

Achieving reliable and precise positional control of DC motors is still a formidable challenge in different engineering disciplines, from industry automation to robotics and mechatronics [4]. Proportional Integral Derivative (PID) controllers are most commonly utilized for this purpose, but their operation is extremely sensitive to the appropriate selection of the control parameters [5]. Classical tuning methods are laborious, lead to less-than-ideal performance, and are rigidly flexible with regard to disturbances, time-variant parameters, and system nonlinearities [6, 7]. Therefore, to improve the dynamic performance and reliability of DC motor position control systems, modern, computerized tuning techniques must be used [8, 9].

This paper introduces an optimized DC motor control system using the Grey Wolf Optimizer (GWO), a soft-computing metaheuristic, to optimize PID controller parameters. The robust GWO algorithm employs grey wolf social hierarchy and predatory behavior to identify the best proportional, integral, and derivative gains. This improves the system's dynamic response compared to traditional optimization methods. The GWO-optimized control loop has been evaluated against various benchmarked optimization methods to prove its effectiveness. Reduced settling time, overshoot, and steady-state stability are the top priorities. Section 1 offers the mathematical modeling of the DC motor and GWO algorithmic formulae, Section 2 examines simulation results and compares data, and Section 3 concludes with research findings.

The GWO approach models the DC motor system more accurately and provides exact industrial automation solutions, according to comparative studies.

Method

A. DC Motor

Electric motors transform electrical energy into mechanical power by producing torque through the interaction of electric current and magnetic coils [10-12]. This process officially begins with the establishment of a magneto-motive force within the motor's magnetic circuit, which subsequently generates the torque required to rotate the rotor. This rotation transforms electrical input into kinetic or mechanical energy [13-18]. Choosing the appropriate motor for a given application is simplified by standardized manufacturer specifications, such as rotational speed, pole count, power capacity, and rated voltage each of which is defined by specific symbols and values [19-21]. Fig. 1 illustrates the basic construction of a DC motor.

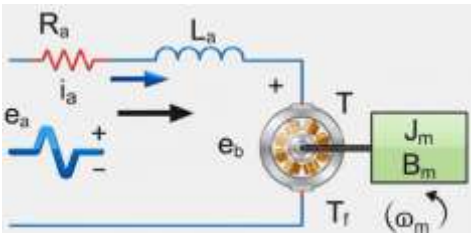

Fig_1. Schematic Diagram of a Basic Model for a DC Motor.

A detailed mathematical model, represented by a set of interconnected differential equations, is used to describe the natural dynamic behavior of a DC motor system.. This analytical model is fundamentally based on the intrinsic topological configuration of the motor's internal circuitry, as illustrated in the schematic diagram in Fig. 1. The

subsequent governing equations are derived by applying Kirchhoff's Voltage Law (KVL) to the principal circuits of the equivalent circuit. This approach simplifies the system to a linear model represented by two main dynamic equations: one for the electrical circuit and one for the mechanical dynamics.

Electrical System Dynamics

Electrical dynamics are governed by applying KVL to the armature circuit, which is represented as a series combination of the armature resistance (R_a), armature inductance (L_a), and the back electromotive force (E_b).

The KVL equation in the time domain is: $E_a(t) = R_a i_a(t) + L_a \frac{di_a(t)}{dt} + E_b(t)$ (1)

Where:

- $E_a(t)$ is the Armature Voltage (the input).
- $i_a(t)$ is the Armature Current.
- R_a is the Armature Resistance.
- L_a is the Armature Inductance.
- $E_b(t)$ is the Back Electromotive Force (Back-EMF).

The Back-EMF is induced in the armature coils as they cut the magnetic flux and is directly proportional to the angular velocity ($\omega(t)$) of the motor shaft:

$$E_b(t) = K_b \omega(t) = K_b \frac{d\theta(t)}{dt} \quad (2)$$

- K_b is the Back-EMF Constant.
- $\omega(t)$ is the Angular Velocity of the shaft.
- $\theta(t)$ is the Angular Position of the shaft.

Mechanical System Dynamics

The mechanical dynamics are governed by Newton's Second Law for rotational motion, which states that the net torque on the rotor equals the moment of inertia times the angular acceleration.

$$T_{net}(t) = J \frac{d\omega(t)}{dt} = \frac{d^2\theta(t)}{dt^2} \quad (3)$$

The net torque is the difference between the torque developed by the motor (T_m) and the opposing torques (friction and external load torque T_L). Assuming the external load torque is negligible ($T_L \approx 0$), the equation becomes:

$$T_m(t) - T_f(t) = J \frac{d\omega(t)}{dt} \quad (4)$$

Where:

- $T_m(t)$ is the Motor Torque (also called Electromagnetic Torque).
- $T_f(t)$ is the Friction Torque.
- J is the Moment of Inertia of the rotor and load.

The Motor Torque is directly proportional to the armature current, under the assumption of a constant magnetic field (constant flux):

$$T_m(t) = K_t i_a(t) \quad (5)$$

K_t is the Motor Torque Constant.

The Friction Torque is typically modelled as viscous friction, which is proportional to the angular velocity:

$$T_f(t) = B\omega(t) \qquad (6)$$

B is the Viscous Friction Coefficient.

Substituting these relations into the net torque equation yields the final mechanical differential equation:

$$K_t i_a(t) - B\omega(t) = J\frac{d\omega(t)}{dt} \qquad (7)$$

The following is a transformation of the system's time-domain mathematical model into the s-domain by using the Laplace transform, assuming zero initial conditions:

$$E_a(s) = (R_a + L_a s)I_a(s) + E_b(s) \qquad (8)$$

Substituting $E_b(s) = K_b\omega(s)$:

$$E_a(s) = (R_a + L_a s)I_a(s) + K_b\omega(s) \;\rightarrow\; I_a(s) = \frac{V_a(s) - K_b\omega(s)}{R_a + L_a s} \qquad (9)$$

Furthermore, the mechanical equation will be as follows:

$$T_m(s) - T_f(s) = Js\omega(s) \qquad (10)$$

Substituting $T_m(s) = K_t\, I_a(s)$ and $T_f(s) = B\omega(s)$:

$$K_t\, I_a(s) - B\omega(s) = Js\omega(s) \;\rightarrow\; K_t\, I_a(s) = (Js + B)\omega(s) \qquad (11)$$

The open-loop block diagram of the DC motor can be constructed from (Eq. 8) through (Eq. 11), as illustrated in Fig. 2:

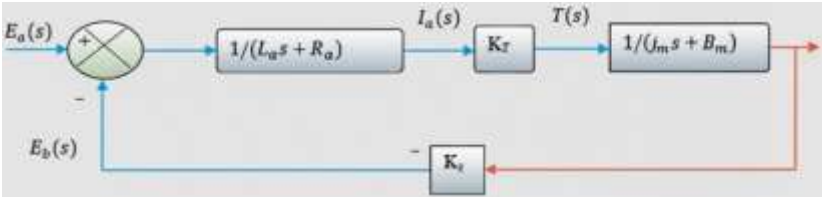

Fig_2. Block Diagram Representation of an Open-Loop DC Motor.

Therefore, the transfer function for position control, $G(s) = \frac{\theta(s)}{V_a(s)}$, is obtained by substituting (Eq. 9) into (Eq. 11) and using the relationship $\omega(s) = s\theta(s)$, which substitutes $\mathrm{I_a(s)}$ from (Eq. 9) into (Eq. 11):

$$K_t\left(\frac{E_a(s) - K_b\omega(s)}{R_a + L_a s}\right) = (Js + B)\omega(s) \qquad (12)$$

$$K_t E_a(s) - K_t K_b\,\omega(s) = (Js + B)(R_a + L_a s)\omega(s) \qquad (13)$$

$$K_t E_a(s) = [(Js + B)(R_a + L_a s) + K_t K_b]\,\omega(s) \qquad (14)$$

$$G(s) = \frac{\omega(s)}{E_a(s)} = \frac{K_t}{L_a Js^2 + (R_a J + L_a B)s + (R_a B + K_t K_b)} \qquad (15)$$

Since $\theta(s) = \frac{1}{s}\,\omega(s)$, therefore, $G(s) = \frac{\theta(s)}{E_a(s)} = \frac{K_t}{s[L_a Js^2 + (R_a J + L_a B)s + (R_a B + K_t K_b)]}$ (16)

B. Design of PID controller

The open-loop transfer function, denoted as $G_\omega(s)$, characterizes the fundamental dynamics of the system. Based on the derivation in (Eq. 16), the transfer function is expressed as:

$$\mathrm{G}(s) = \frac{K}{a_3 S^3 + a_2 S^2 + a_1 S} \qquad (17)$$

Where the constant parameters are defined by the physical attributes of the motor: $K = K_t$, $a_3 = L_a J$ $a_2 = L_a J + L_a B$, $a_1 = R_a B + K_t K_b$. To govern this system, a PID controller is employed, with its transfer function defined as:

$$C(s) = K_P + \frac{K_P}{s} + K_D S \qquad (18)$$

According to (Eq. 15), the actual output displacement $\theta(s)$ is a function of the input voltage $E_a(s)$ and the plant $G(s)$. To achieve the target rotation, the input voltage must be precisely regulated. The procedure is implemented by introducing a reference input $\theta_d(s)$ and integrating a feedback controller, as illustrated in the closed-loop block diagram of Fig. 3.

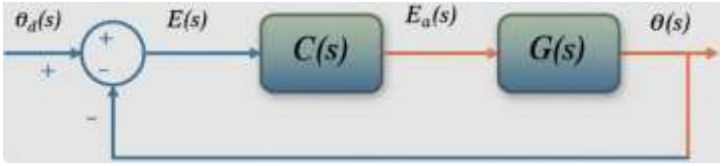

Fig_3. Block Diagram Representation of a Closed-Loop DC Motor.

The overall behavior of the system is described by the closed-loop transfer function $T(s)$, which represents the ratio of the output displacement to the desired reference $T(s) = \frac{\theta(s)}{\theta_d(s)}$, From the feedback structure shown in Fig. 3, the relationship can be written as:

$$[\theta_d(s) - \theta(s)]C(s)G(s) = \theta(s) \qquad (19)$$

Solving for the transfer function $T(s)$ yields:

$$T(s) = \frac{\theta(s)}{\theta_d(s)} = \frac{C(s)G(s)}{1+C(s)G(s)} \qquad (20)$$

The closed-loop operation block can be reconstructed from Eq. (18) to Eq. (20). and it's demonstrated in Fig. 4.

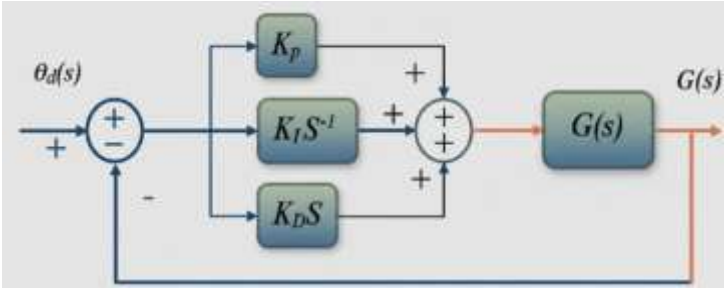

Fig_4. Block diagram illustration of a PID-controlled DC motor.

By substituting the PID controller components from (Eq. 12) into the general control block, the detailed architecture for the DC-motor control is represented in Fig. 4. Consequently, the relationship is expanded as follows:

$$[\theta_d(s) - \theta(s)]\left[K_P + \frac{K_I}{S} + K_D\right]\frac{K}{a_3S^3+a_2S^2+a_1S} = \theta(s) \qquad (21)$$

Through algebraic manipulation of (Eq. 21), the final closed-loop transfer function for the DC-motor system is obtained:

$$T(s) = \frac{\theta(s)}{\theta_d(s)} = \frac{K[K_D S^2+K_P S+K_I]}{a_3S^4+a_2S^3+a_1S^2+KK_DS^2+KK_PS+KK_I} \qquad (22)$$

C. GWO-Based PID Controller

Fig. 5 shows a diagram of how the GWO's social structure works. The goal of this social group is to act like wolves in the wild when they obtain food and become leaders [22]. The Alpha (α) is the highest rank in this system, which is why it is known as the apex position. They are the ones who make the most crucial decisions and watch how the flock moves and hunts. [22, 23] indicates that the Beta (β) is tasked with supporting the Alpha in executing commands and is likely to assume leadership once the Alpha has fulfilled their roles. The third stratum, designated as the Delta (δ), consists of subordinates, including observers and sentinels, who carry out the directives of superior ranks while overseeing the fundamental level of the pack [24]. At the bottom of the hierarchy, the Omega (ω) holds the lowest rank. It is the lowest rank, positioned beneath all other ranks, yet it plays a crucial role in maintaining the stability of the pack [25]. The workflow flowchart in Fig. 5 [26] provides an additional overview of this group intelligence and organizational process, which occurs from the first search to the choice of the best parameters.

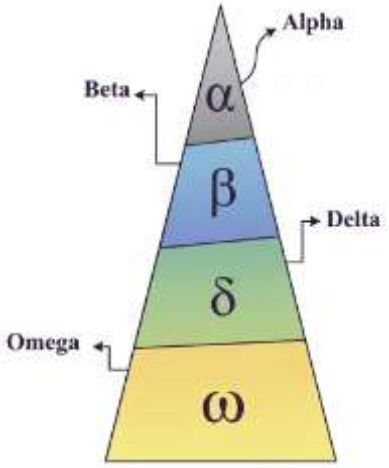

Fig_5. Schematic Representation of the Social Hierarchy within GWO.

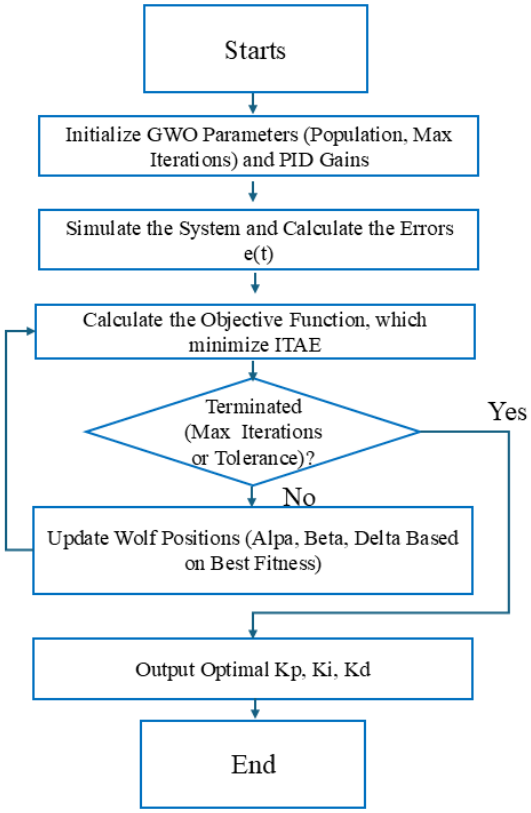

Fig_6. GWO-PID Flow Chart.

The GWO, as proposed by Mirjalili et al. (2014) [8], models the social hierarchy and foraging strategies of grey wolves through a sequence of iterative mathematical procedures. The procedure commences with Encircling Prey, during which wolves revise their positions relative to the target, and after that, they attack; these behaviors are dictated by two main vector equations, respectively:

$$D = \left|C.X_p(t) - X(t)\right| \quad (23)$$

$$X(t+1) = X_p(t) - A.D \quad (24)$$

Where:

- D is the distance vector between a wolf and the prey.
- $X_p(t)$ is the location of prey (representing the current optimal solution).
- $X(t)$ is the current position of the grey wolf.
- C is a stochastic weight coefficient vector.
- A is a convergence vector governing the incremental adjustment magnitude.
- $X(t+1)$ is the wolf's new location.

In accordance with the above-described algorithm, the initial step of the PID controller optimization procedure is determined by specifying the subsequent parameters:

- Random lower bounds for PID parameters [K_{P_1}, K_{I_1}, K_{D_1}].

- Random upper bounds for PID parameters [K_{P_n}, K_{I_n}, K_{D_n}].

- Maximum number of iterations n.

- Size of population size, denoted as P.

- Inertial weights w1, w2, and w3.

Initializing the population's placements inside the search space is the next step in the method after parameter initialization. To determine the Alpha, Beta, and Delta leaders, the third step is evaluating the designated objective function for each grey wolf, which the wolves with the first, second, and third lowest costs are designated as α , β, and δ, respectively. Objective function can be calculated by using Eq (25) as follows:

$$E = w_1(E_{os}) + w_2E_{pt} + w_3E_{rs} \quad (25)$$

where E_{pt} is the peak time error, E_{rs} is the rise time error, and E_{os} is the percentage overshoot error. These errors are computed based on the absolute difference between the desired and actual responses.

The fourth step is encircling the prey, for which the wolves begin to converge on the best solutions found. The fifth step is when the ω wolf updates its position based on the positions of the α, β, and δ wolves; this step can be defined as a hunting and position updating. The final step is repeating, as is the algorithm, which continues the loop of evaluating and updating until a stopping condition is met.

The output of the system is quantified using four specific performance indices, with a primary focus on the Integral Time Absolute Error (ITAE) and the Integrated Absolute Error (IAE). These indices, defined in (Eq. 26) and (Eq. 27), respectively, are integrated into the cost function as follows:

$$ITAE = \int_0^\infty t|e(t)|dt \quad (26)$$

$$IAE = \int_0^\infty |e(t)|dt \quad (27)$$

Alternative criteria to the objective function include the Integration of Squared Error (ISE), the Integration of Time-weighted Squared Error (ITSE) [27].

The system response that aligns with the performance specifications corresponding to the minimum value of the objective function signifies the optimal response.

The wolves that produce that response are regarded as the optimal set of values for the PID controller gains.

Results and Discussion

The computation of the response of the DC motor uses different system properties. These properties are tabulated in Table 6.1. This computation is used to estimate how well the motor responds [28].

Table-1 DC motor parameters.

Symbol	Quantity	Value	Unit
R_a	Armature Resistance	2.45	Ω
L_a	Armature Inductance	0.035	H
K_t	Torque Constant	1.2	$N.m/A$
K_b	Back-EMF Constant	1.2	$V/(rad/sec)$
J	Moment of Inertia of Rotor	0.022	$Kg.m^2$
b	Viscous Friction Coefficient	0.0005	$N.m/(rad/sec)$

The investigated system's mathematical model has been simulated as optimized systems. In other words, optimized closed loop responses are assessed based on the outcomes. The responses are provided only for the rotary displacement (rad) of the motor position. The DC motor is analyzed by implementing MATLAB to the equations in Section 2, where GWO was employed to optimize the PID controller parameters K_P, K_I, K_D for a DC motor. The primary objective was to minimize a cost function based on the error between the system's actual time-domain response and a set of strict desired specifications. The optimization process was initialized with a population size of 12 wolves and a maximum iteration limit of 150.

The algorithm demonstrated robust convergence characteristics, successfully minimizing the objective function to a value of 0.0393, which is below the pre-defined stoppage criterion of 0.04. This indicates that the algorithm successfully located a global or near-global optimum within the search space.

The optimized system performance achieved via the GWO algorithm is illustrated in Fig. 7. These results highlight the specific transient characteristics obtained when the GWO-optimized parameters are applied to the controller. By illustrating how the algorithm governs system positioning, this Fig. provides essential insights necessary for the continued analysis and optimization of the control system. The performance of the optimized PID controller was evaluated using a unit step response simulation. The resulting system characteristics were analyzed against the desired design requirements.

The system's performance is looking solid and aligns closely with our design goals. The attained maximal overshoot (M_p) was 10.0062%, demonstrating close agreement with the intended target of 10%. The response was also impressively quick, settling (T_s) within 0.2229 S, comfortably beating the 0.25 S requirement while reaching its peak value (T_p) at 0.1560 S.

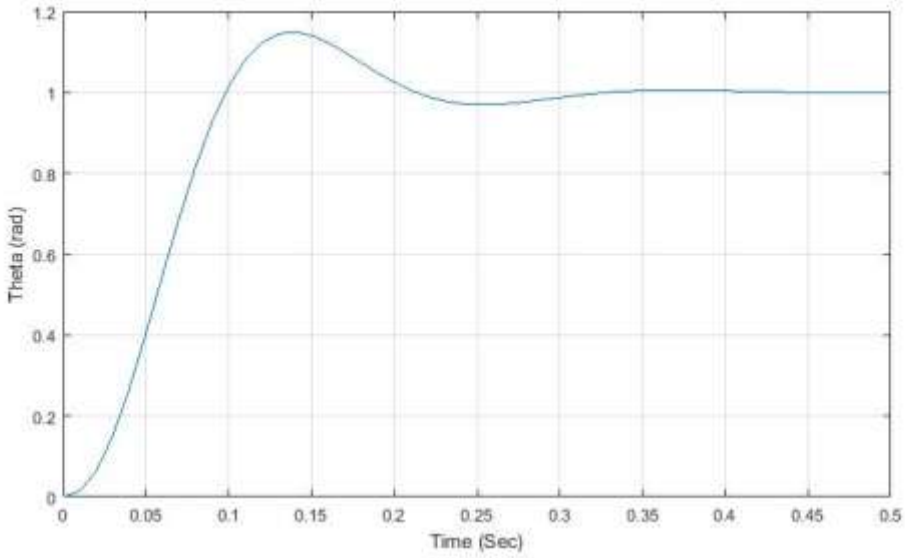

Fig_6. Optimized System Response based on GWO.

To validate the effectiveness of the proposed approach, the simulation results were compared with the results reported in the reference study [28,29]. A comparison of the Desired Targets, the Proposed Method (GWO), and the Reference Papers are presented in Table 2.

Table-2 The performance of GWO, PSO, and GA was Evaluated by Comparing their Actual Responses Against the Required Specifications.

Desired Response			GWO Response			PSO Response			GA Response		
P.O	**S.T**	**P.T**	**P.O**	**S.T**	**P.T**	**P.O**	**S.T**	**P.T**	**P.O**	**S.T**	**P.T**
10	0.25	0.15	10.00	0.222	0.156	10.03	0.210	0.149	5.09	0.204	0.154
15	0.25	0.15	15.00	0.281	0.135	14.99	0.278	0.134	11.1	0.230	0.162
20	0.30	0.15	20.00	0.286	0.129	20.00	0.283	0.130	14.6	0.279	0.135
22	0.30	0.15	22.00	0.291	0.131	22.01	0.282	0.127	16.9	0.298	0.140

Based on the results demonstrated in the table, the errors were calculated according to the required system responses by computing the absolute errors between the actual and required responses for the four records. These responses, generated using GA, PSO, and GWO techniques, are further detailed in Table-3, which shows the errors in the percentage overshoot, settling time, and peak time; consequently, the average error was also calculated to evaluate the feasibility of these applied optimization techniques and to benchmark the performance of the GWO approach against the the established GA and PSO frameworks.

Table-3 Absolute Percentage Errors for GWO, PSO, and GA System Responses.

	Absolute Percent Error GA			Absolute Percent Error PSO			Absolute Percent Error GWO		
	E.P.T	**E.S.T**	**E.P.O**	**E.P.T**	**E.S.T**	**E.P.O**	**E.P.T**	**E.S.T**	**E.P.O**
	0.004	0.046	4.91	0.001	0.04	0.03	0.006	0.028	0
	0.012	0.02	3.9	0.016	0.028	0.01	0.015	0.031	0
	0.015	0.021	5.4	0.02	0.017	0	0.021	0.014	0
	0.01	0.002	5.1	0.023	0.018	0.01	0.019	0.009	0
Average Error	0.0102	0.0222	4.8275	0.015	0.0257	0.0125	0.0152	0.020	0
Toatal Average Error		**1.62**			**0.0177**			**0.0119**	

The performance indices obtained from the simulation demonstrate a clear advantage for GWO over the established GA and PSO benchmarks. By analyzing the transient response, it becomes evident that GWO minimizes the trade-off between speed and stability. While GA and PSO exhibit higher oscillations and slower recovery times, GWO maintains a tighter grip on the setpoint. This leads to a marked reduction in both settling time and steady-state error.

The following results highlight how the hierarchical search mechanism of GWO suppresses overshoot more effectively than the reference methods. These improvements are quantified through the error indices calculated below, proving that GWO offers superior damping and precision. The numerical comparison of these key performance indicators is summarized in Table-4 below.

Table-4 Comparison of Error Indices and Percentage Improvement for GA, PSO, and the Proposed GWO

Method	Avg. Error (e)	IAE	ITAE	Improvement (%)
GA	1.6200	5.23	22.4	Benchmark
PSO	0.0178	4.8	18.15	8.20%
GWO	0.0119	2.1	12.45	59.80%

Conclusion

The results of this study really highlight why the GWO is such a strong choice for optimizing DC motor controllers, especially when compared to more traditional methods. The most striking takeaway is the performance gap between GWO and more conventional metaheuristic techniques; specifically, the GWO approach demonstrated a 59.80% improvement over the GA and maintained an 8.20% performance lead over PSO. By achieving a maximum overshoot of 10.0062% virtually hitting the 10% design target and maintaining a negligible average error of 0.0119, the proposed method successfully resolves the common tension between system speed and steady-state stability.

Given these findings, future research should prioritize physical hardware validation to see how the GWO-tuned parameters hold up against real-world factors like sensor noise, heat dissipation, and mechanical friction. It is also recommended that subsequent studies evaluate the controller's resilience under fluctuating load conditions or investigate hybrid strategies, such as a combined GWO-PSO algorithm, to potentially reach even higher levels of precision in high-stakes industrial applications.

Compliance with ethical standards

Disclosure of conflict of interest

The authors declare that they have no conflict of interest.

References

[1] Gaing, Z. L. (2004). A particle swarm optimization approach for optimum design of PID controller in AVR system. IEEE Transactions on Energy Conversion, 19(2), 384-391.

[2] Solihin, M. I., Tack, L. F., & Kean, M. L. (2011). Tuning of PID controller using particle swarm optimization (PSO). International Journal of Advanced Science, Engineering and Information Technology, 1(4), 458-463.

[3] [3] Bingul, Z., & Karahan, O. (2011). A fuzzy logic controller tuned with particle swarm optimization for 2 DOF robot trajectory control. Expert Systems with Applications, 38(1), 1017-1031.

[4] Yazgan, H., Yener, F., & Soysal, S. (2019). Comparison Performances of PSO and GA to Tuning PID Controller for the DC Motor. Sakarya University Journal of Science, 23(2), 162-174.

[5] Thomas, N., & Poongodi, P. (2016). Position control of DC motor using genetic algorithm based PID controller. Proceedings of the IEEE International Conference on Recent Trends in Information Technology (ICRTIT).

[6] Borase, R. P., Maghade, D. K., Sondkar, S. Y., & Pawar, S. N. (2021). A review of PID control, tuning methods and applications. International Journal of Dynamics and Control, 9(2), 818-827.

[7] Jaen-Cuellar, A., et al. (2013). PID-Controller Tuning Optimization with Genetic Algorithms in Servo Systems. International Journal of Advanced Robotic Systems, 10(9).

[8] Mirjalili, S., Mirjalili, S. M., & Lewis, A. (2014). Grey Wolf Optimizer. Advances in Engineering Software, 69, 46-61.

[9] Pandey, S., et al. (2024). Modern Optimization Techniques Based PID Controller Tuning for the Speed Control of a DC Motor. ResearchGate.

[10] Trong Duy Nguyen, King-Jet Tseng, Shao Zhang, and Hoan Thong Nguyen, "A novel axial flux permanent-magnet machine for flywheel energy storage system: Design and analysis," IEEE Transactions on Industrial Electronics, vol. 58, no. 9, pp. 3784–3794, Sep. 2011, doi: 10.1109/TIE.2010.2089939.

[11] L. Peng, L. Ma, W. Song, and H. Liu, "A simple model predictive instantaneous current control for single-phase pwm converters in stationary reference frame," *IEEE Transactions on Power Electronics*, vol. 37, no. 7, pp. 7629–7639, Jul. 2022.

[12] A. K. K. A. Raheem, S. W. Shneen, M. H. Jaber, and A. H. Reja, "Design and simulation of a second-order universal switched-capacitor filter as a 10-pin dual-in-line package integrated circuit," *Engineering and Technology Journal*, vol. 30, no. 18, pp. 3175–3191, 2012.

[13] C. Reeves, *Modern Heuristic Techniques for Combinatorial Problems*. 1993.

[14] S. W. Shneen, A. Z. Salman, Q. A. Jawad, and H. Shareef, "Advanced optimal by pso-pi for dc motor," *Indonesian Journal of Electrical Engineering and Computer Science*, vol. 16, no. 1, pp. 165–175, 2019.

[15] S. W. Shneen, H. S. Dakheel, and Z. B. Abdulla, "Design and implementation of variable and constant load for induction motor," *International Journal of Power Electronics and Drive Systems*, vol. 11, no. 2, pp. 762–773, 2020.

[16] S. W. Shneen, M. Q. Sulttan, and M. H. Jaber, "Variable speed control for 2Ph-HSM in RGS: A comparative simulation study," *International Journal of Electrical and Computer Engineering*, vol. 10, no. 3, pp. 2285–2295, 2020.

[17] F. A. Silaban, S. Budiyanto, and W. K. Raharja, "Stepper motor movement design based on FPGA," *International Journal of Electrical and Computer Engineering*, vol. 10, no. 1, pp. 151–159, 2020.

[18] R. Thangaraj, T. R. Chelliah, M. Pant, A. Abraham, and C. Grosan, "Optimal gain tuning of PI speed

controller in induction motor drives using particle swarm optimization," *Logic Journal of IGPL*, vol. 19, no. 2, pp. 343–356.
[19] J. Wang, G. Zhang, H. Zhang, and T. Fuhlbrigge, "Force control technologies for new robotic applications," in *2008 IEEE International Conference on Technologies for Practical Robot Applications, TePRA*, 2008, pp. 143–149,.
[20] W. K. Wibowo and S. K. Jeong, "Genetic algorithm tuned PI controller on PMSM simplified vector control," *Journal of Central South University*, vol. 20, no. 11, pp. 3042–3048, 2013.
[21] E. M. Ismaeil, M. S. Zaky, and M. M. Khater, "DSP-Based real-time control of a two phase hybrid stepping motor," *Journal of Electrical Engineering*, vol. 10, no. 4, p. 6, 2010.
[22] Mirjalili, S., Mirjalili, S. M., & Lewis, A. (2014). Grey wolf optimizer. *Advances in Engineering Software*, 69, 46-61.
[23] Muro, C., Escobedo, R., Spector, L., & Coppinger, R. P. (2011). Wolf-pack (Canis lupus) hunting strategies emerge from simple rules in computational simulations. Behavioural Processes, 88(3), 192-197.
[24] Faris, H., Aljarah, I., Sayed, G. I., & Mirjalili, S. (2018). Grey wolf optimizer: a review of recent variants and applications. Neural Computing and Applications, 30(2), 413-435..
[25] Gupta, S., & Deep, K. (2019). A novel self-adaptive grey wolf optimizer based on low-discrepancy sequence. Expert Systems with Applications, 113, 177-192.
[26] Saremi, S., Mirjalili, S., & Lewis, A. (2017). Grasshopper optimisation algorithm: Theory and application. *Advances in Engineering Software*, 105, 30-47.
[27] Wu, Z., Signal de-noising method based on particles swarm algorithm and wavelet transform. Technical gazette, Vol 21, No.5 pp. 1001-1009, 2014.
[28] Bindu, R., & Namboothiripad, M. K., Tuning of PID controller for Dc-servo motor using genetic algorithm. International Journal of Emerging Technology and Advanced Engineering, Vol 2, No.3 pp. 310-314, 2012.
[29] Adel Agila, Aysha Ali, and Babak D. Rouyendeg, OPTIMAL POSITION CONTROL OF A MORE COMPLICATED SYSTEM BASED ON OPTIMIZATION TECHNIQUES. AL-MUKHTAR JOURNAL OF ENGINEERING RESEARCH, Vol.1, No. (4): 80-87,2021.

